Phase transitions and polarization switching in quasi-one-dimensional organic ferroelectrics of the phenyltetrazole family

A. P. Moina*
Yukhnovskii Institute for Condensed Matter Physics, 1 Svientsitskii St., 79011 Lviv, Ukraine

(Received 30 September 2025; revised 23 November 2025; accepted 25 November 2025; published 15 December 2025)

Pseudospin models are proposed for the description of the phase transitions, dielectric characteristics, and polarization switching in two crystals of the phenyltetrazole family. One of them, APHTZ, is a canted ferroelectric, whereas the other, MPHTZ is a simple antiferroelectric. In APHTZ, the electric field, applied perpendicularly to the axis of spontaneous polarization, flips the polarization in one of the two sublattices, effectively rotating the nonzero net polarization by 90° and switching the system between two different ferroelectric configurations. The temperature-electric field phase diagrams are constructed. The diagram topology appears to be typical for the Ising-like antiferroelectric systems.

DOI: 10.1103/cf7x-szr4

I. INTRODUCTION

There is currently much interest [1] in the search for lead-free organic ferroelectric and antiferroelectric systems as promising technologically advantageous candidates for various applications, like high-energy-storage capacitors.

It has been very recently discovered [2] that organic crystals of the 5-phenyl-1*H*-tetrazole (PHTZ) family exhibit ferroelectric (FE), antiferroelectric (AFE), or phase mixture FE/AFE or AFE/AFE behavior. Amongst several studied crystals of this family, two, 5-(4-methylphenyl)-1*H*-tetrazole (MPHTZ) and 5-(4-aminophenyl)-1*H*-tetrazole (APHTZ) were found to have a long-range order. APHTZ appears to be a canted ferroelectric with FE ordering along the *a* axis that coexists with the AFE ordering along the *b* axis [2]. MPHTZ is a simple uniaxial AFE. The ordered phases are stable at least up to 410 K.

The common feature and the building blocks of the structure of all PHTZ crystals are pentagonal heterocyclic tetrazole (CN_4) groups, hydrogen bonded into quasi-one-dimensional chains, as shown in Fig. 1. The radicals *R*, linked to the C atoms of tetrazole groups via phenyl rings, are different in different crystals: $R = NH_2$ in APHTZ and CH_3 in MPHTZ. The crystals with $R = Cl$ and $R = F$ exhibit a mixture of FE/AFE ordering due to the nearly degenerate ground states with very close energies of the FE and AFE configurations [2]. The parent PHTZ compound ($R = H$) has been identified as an AFE/AFE phase mixture, where different AFE configurations have close energies.

Dynamics of the dipole moments in PHTZ crystals and their switching by external electric field are a perfect example of proton tautomerism. Protons of the NH···N hydrogen bonds move in double-well potentials. The positions of switchable double electron bonds (the π bonds between one of the two N–C pairs of each tetrazole group) and the directions of the dipoles to be associated with each molecule are determined by the positions of the protons on the linking hydrogen bonds. As illustrated in Fig. 1, the relocation of each proton to the other site along each hydrogen bond switches the π bonds to the other N–C pairs in the groups, as well as flips all dipoles and the chain polarization. This polarization, according to the Berry phase calculations [2], is almost equally formed by the switchable π bonds and by the ionic displacements.

Switching of a sublattice polarization by the external electric field and the resulting transition from the AFE to FE phase is a signature feature of antiferroelectrics. In uniaxial AFEs, the polarization flips by 180° at once, which is revealed as a classical double *P*-*E* hysteresis loop. In multiaxial AFEs, like squaric acid [3–5] or CPPLA [6], the loops are quadruple, because of the two-step polarization rotation. MPHTZ, being a uniaxial AFE, exhibits a classical switching process [2]. APHTZ, being a canted FE, possesses compensated dipole moments along the *b* axis. Thus, it potentially should also exhibit polarization switching: the electric field applied along the *b* axis can flip the dipoles in one of the sublattices, inducing a transition to the state, where the ordering is FE along the *b* axis and AFE along the *a* axis. In APHTZ, one thus expects to observe a single FE loop for the field along the *a* axis and a double loop for the field applied along the *b* axis.

Theoretical model description of the phase transitions and polarization switching in the systems with proton tautomerism is often based [4,5,7] on a certain version of the pseudospin proton ordering model. Since the pioneering works by Blinc [8] and de Gennes [9], similar Ising-type models, possibly modified by inclusion or neglecting proton tunneling, coupling to phonons or to macroscopic lattice strains, have been extensively and successfully used to describe the temperature,

*Contact author: alla@icmp.lviv.ua

Published by the American Physical Society under the terms of the Creative Commons Attribution 4.0 International license. Further distribution of this work must maintain attribution to the author(s) and the published article's title, journal citation, and DOI.

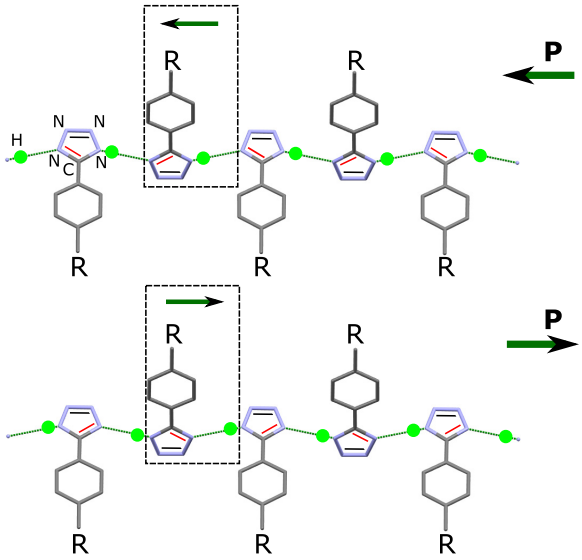


FIG. 1. Two fully ordered hydrogen-bonded 5-(4-*R*-phenyl)-1*H*-tetrazole chains with opposite polarizations. Switchable and nonswitchable π bonds of tetrazole groups are shown in red and black, respectively. The dashed rectangles outline the unit that will be treated as a switchable dipole in the proposed models (see next Section).

external mechanical stress or electric field behavior of the static dielectric, piezoelectric, elastic, thermal, as well as dynamic properties of numerous hydrogen bonded ferroics (see, e.g., Refs. [4,5,7,10–16] and references therein). The apparent bistability of the proton-associated dipoles in the PHTZ family crystals will enable us to use the pseudospin formalism, and the quasi-one-dimensional structure of the dipole chains will make such calculations particularly simple. To our best knowledge, no such description for these crystals has been carried out yet.

In the present paper, we consider the two crystals of this family, which exhibit the long-range ordering: APHTZ and MPHTZ. Our goal is to develop as simple as possible pseudospin models, which would reproduce the essential features of the structure, type of ordering, available experimental data for the physical characteristics of the real crystals, and which would use as few fitting parameters as possible. The processes of polarization switching in these crystals are another focus of our attention.

II. APHTZ

The monoclinic (space group *Pn*) APHTZ crystals have a layered-like structure, where each layer is formed by the illustrated in Fig. 1 parallel chains of molecules, linked by hydrogen bonds. As seen in Fig. 2, the layers are stacked along the *c* axis, and the chains are alternatingly (from layer to layer) directed either along [110] or [1$\bar{1}$0]. The dipole moment of each molecule thus has both *a* and *b* components, and different types of the long-range order along the two directions are possible.

According to the DFT calculations of Ref. [2], the energy of the APHTZ system is lowest in the configuration, where the ordering is FE along the *a* axis and AFE along the *b*

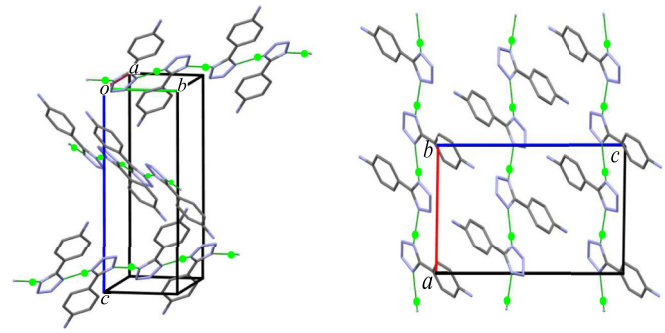


FIG. 2. Two projections of the crystal structure of APHTZ, visualized [17] using the x-ray data of Ref. [2]. Hydrogen bonds, linking the tetrazole groups, are shown in green; the other hydrogen atoms are hidden for clarity. The off-center displacements of protons along these bonds are exaggerated. The FE-I configuration is depicted (see text).

axis (the shown in Fig. 2 fully ordered FE-I configuration [2]). In this configuration, all the protons are ordered in the furthermost (along the *a* axis) of the two equilibrium sites on each hydrogen bond, linking the tetrazole groups. The hysteresis measurements [2] also confirmed the ferroelectric ordering along the *a*-axis in APHTZ.

The proposed model is shown in Fig. 3. It consists of stacked along the *c* axis parallel layers, each formed by parallel chains of dipoles. All chains are going along [110] in the odd layers (sublattice $s = 1$) and along [1$\bar{1}$0] in the even layers (sublattice $s = 2$). Each effective dipole is associated with a tetrazole group and the proton, moving in the two-well potential on the hydrogen bond attached to the rightmost (along the *a* axis) N atom of the group. The dipole moment is formed by ionic displacements and by the switchable π bond of the group. Its direction coincides with the direction of the proton shift relative to the center of the hydrogen bond (see also Fig. 1). When the proton relocates from one equilibrium site on the hydrogen bond to the other, the entire dipole flips by 180°.

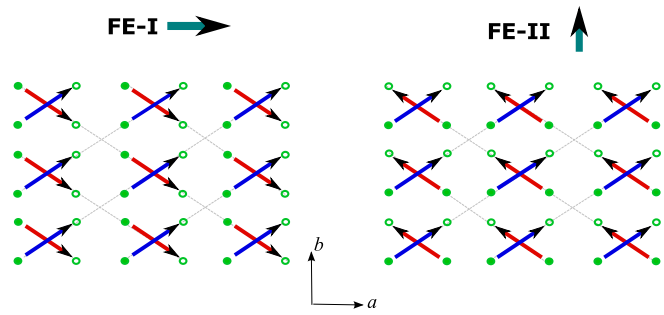


FIG. 3. Fully ordered configurations FE-I and FE-II of the APHTZ model (see text and Ref. [2]). Two layers of parallel chains of dipoles oriented along [110] (blue arrows, sublattice $s = 1$) and [1$\bar{1}$0] (red arrows, sublattice $s = 2$) are shown for each configuration. Full and open green circles are the occupied and vacant proton sites on each hydrogen bond. Large green arrows indicate the net polarization directions. The dipole sizes and relative distances between the sites, chains, etc. are schematic only and do not reflect the real ones.

In the FE-I configuration (Fig. 3, left), all the dipoles point in the positive direction along the a axis, whereas their projections on the b axis alternate between the layers and are thus compensated: the system is FE along the a axis and AFE along the b axis. Another possibility is the FE-II configuration (Fig. 3, right), with the FE order along the b axis and AFE order along the a axis. The energy of this configuration was found [2] to be higher than that of FE-I. It is expected that the electric field E_b can induce a switching from phase FE-I to phase FE-II.

Due to the obvious bistability of each ordering element of the model (the proton in a double-well potential and the associated electric dipole), the pseudospin formalism is most preferable for the calculations. Motion of a proton is described by an Ising pseudospin, whose two eigenvalues $\sigma = \pm 1$ are assigned to the two equilibrium proton sites on the bond. We assume that $\sigma = 1$, if the proton sits at the right site (along the a axis), and the associated dipole points to the right, and $\sigma = -1$ if the proton sits at the left one, and the dipole points to the left (see Figs. 1 and 3).

The model Hamiltonian includes pairwise long-range interactions between the dipoles, as well as the energy of their interactions with external electric fields E_a and E_b

$$H = -\frac{1}{2}\sum_{s,s'=1,2}\sum_{ff'} J_{\substack{sf\\ s'f'}}\frac{\sigma_{sf}}{2}\frac{\sigma_{s'f'}}{2} - \mu_a E_a \sum_{s=1,2}\sum_{f}\frac{\sigma_{sf}}{2} - \mu_b E_b\left[\sum_{f\in 1}\frac{\sigma_{1f}}{2} - \sum_{f\in 2}\frac{\sigma_{2f}}{2}\right]. \tag{1}$$

The summations go over two sublattices ($s = 1, 2$) and sites f belonging to the sublattice s (f is a combined index, which includes the indices of the layer in the sublattice, of the chain within the layer, and of the site within the chain).

The simplest mean-field approximation shall be used for Hamiltonian (1). Considering the symmetry of the model, there are two different order parameters, one for each of the sublattices

$$\langle\sigma_{sf}\rangle = \eta_s.$$

In the absence of an external field, $\eta_1 = \eta_2$ for the FE-I configuration and $\eta_1 = -\eta_2$ for the FE-II configuration.

In the mean-field approximation,

$$H = NH_0 - \sum_{f\in 1} h_1\frac{\sigma_{1f}}{2} - \sum_{f\in 2} h_2\frac{\sigma_{2f}}{2}, \tag{2}$$

where N is the total number of dipoles in each sublattice;

$$H_0 = \tfrac{1}{8}\left[J_{11}\eta_1^2 + 2J_{12}\eta_1\eta_2 + J_{11}\eta_2^2\right], \tag{3}$$

and

$$h_1 = \frac{J_{11}\eta_1 + J_{12}\eta_2}{2} + \mu_a E_a + \mu_b E_b,$$
$$h_2 = \frac{J_{12}\eta_1 + J_{11}\eta_2}{2} + \mu_a E_a - \mu_b E_b \tag{4}$$

are the mean fields acting on the pseudospins of the sublattices 1 and 2, respectively. The intra- and intersublattice interaction constants $J_{ss'}$

$$J_{11} = \sum_{f'\in 1} J_{\substack{1f\\ 1f'}} = \sum_{f'\in 2} J_{\substack{2f\\ 2f'}},$$
$$J_{12} = \sum_{f'\in 2} J_{\substack{1f\\ 2f'}} = \sum_{f'\in 1} J_{\substack{2f\\ 1f'}} \tag{5}$$

represent the total action exerted by all pseudospins of the sublattice s' on each pseudospin of sublattice s. Depending on the sign of J_{12} at positive J_{11}, Hamiltonian (2) can predict either FE-I or FE-II configuration as the ground state at $E_b = 0$.

Calculation of the thermodynamic potential is straightforward, yielding

$$g = \frac{G}{N} = H_0 - \frac{1}{\beta}\ln 2\cosh\frac{\beta h_1}{2} - \frac{1}{\beta}\ln 2\cosh\frac{\beta h_2}{2}, \tag{6}$$

where $\beta = (k_B T)^{-1}$. Minimizing it with respect to the order parameters η_1 and η_2, we obtain the following equations for them

$$\eta_s = \tanh\frac{\beta h_s}{2}, \tag{7}$$

which form is typical for the mean-field approximation. Equally straightforward is to find crystal polarizations $P = -v^{-1}\frac{\partial g}{\partial E}$ along the a and b axes

$$P_a = \frac{\mu_a}{2v}(\eta_1 + \eta_2),$$
$$P_b = \frac{\mu_b}{2v}(\eta_1 - \eta_2);$$

$v = 364$ Å^3 is the crystal volume per two formula units [2].

From here, we derive explicit expressions for the dielectric permittivities of the system in the FE-I configuration for zero bias fields

$$\varepsilon_i = \frac{1}{\varepsilon_0}\frac{\partial P_i}{\partial E_i} = \frac{\beta\mu_i^2}{2\varepsilon_0 v\varphi_i}, \tag{8}$$

where ε_0 is the dielectric permittivity of a free space, i is either a or b, and

$$\varphi_{a,b} = \frac{1}{1-\eta_0^2} - \frac{\beta(J_{11}\pm J_{12})}{4}. \tag{9}$$

Here $\eta_0 \equiv \eta_1 = \eta_2$ is the spontaneous order parameter. In the paraelectric phase ($\eta_0 = 0$), both permittivities obey the Curie-Weiss law with the Curie-Weiss temperatures

$$T_{a,b}^{\mathrm{CW}} = \frac{J_{11}\pm J_{12}}{4k_B}. \tag{10}$$

Before going into the numerical calculations, the following disclaimer should be made. The fitting procedure for PHTZ crystals is complicated by a severe deficit of experimental data, like the value of the transition temperature, or the temperature curves of spontaneous polarization and static permittivity, usually available for ferroelectric crystals. The chosen values of the fitting parameters are preliminary and must be adjusted when additional data become available.

First, it is obligatory that $J_{11} > 0$ to ensure the FE ordering and absence of modulation within each sublattice. The further choice of the model parameters is based on the assumption

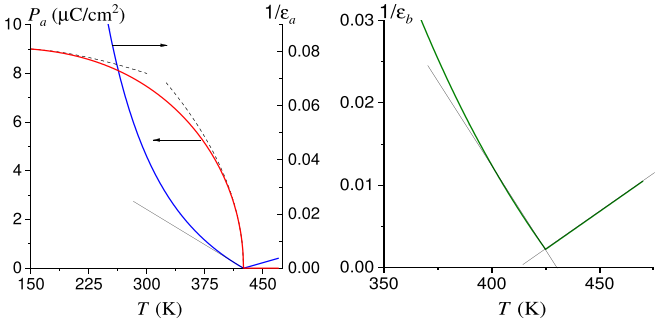


FIG. 4. The temperature dependences of the spontaneous polarization $P_a = \mu_a \eta_0 / v$, inverse dielectric permittivities ε_a^{-1} (left) and ε_b^{-1} (right) of APHTZ. Dashed lines: P_a calculated with η_0 approximated according to Eqs. (12) and (13).

that the ground state of the system is FE-I. In this case, we must put $J_{12} > 0$.

The temperature and field-dependent equilibrium values of the order parameters η_s are found by direct minimization of the thermodynamic potential (6) and required to obey Eqs. (7). When both J_{11} and J_{12} are positive and $E_b = 0$, the system behavior is governed by two model parameters: the sum $J_{11} + J_{12}$, irrespectively of the J_{11} to J_{12} ratio, and the effective dipole moment μ_a. It is known [2] that the ferroelectric phase is stable at least up to 410 K. Using the Curie-Weiss temperature T_a^{CW} as an estimate for T_c, from Eq. (10) it then follows that $(J_{11} + J_{12})/k_{\mathrm{B}}$ should exceed 1640 K. We use $(J_{11} + J_{12})/k_{\mathrm{B}} = 1700\,\mathrm{K}$, which sets the transition temperature to 425 K.

The value of effective dipole moment $\mu_a = 3.3 \times 10^{-29}$ C m is chosen to yield the spontaneous polarization $P_a = 7.5$ μC/cm^2 at 300 K in agreement with the value obtained by the Berry phase calculations and with the measured value 7.0 μC/cm^2 of the remanent polarization at 300 K [2]. Note that normal FE-type (single) hysteresis loops P_a-E_a were observed [2].

Figure 4 (left) shows the calculated temperature dependence of the spontaneous polarization P_a and the inverse static dielectric permittivity ε_a of the APHTZ crystal. As expected, the developed model predicts a second-order phase transition, so the transition temperature T_c at zero field coincides with the Curie-Weiss temperature T_a^{CW} and is given by Eq. (10) exactly:

$$T_c = \frac{J_{11} + J_{12}}{4k_{\mathrm{B}}}. \tag{11}$$

It is well known and can be easily shown by expanding the right-hand side (r.h.s.) of Eqs. (7) that at temperatures close to T_c the spontaneous order parameter η_0 can be presented as

$$\eta_0 = \sqrt{3\frac{T_c - T}{T_c}}. \tag{12}$$

On the other hand, at low temperatures η_0 approaches saturation and can be approximated as

$$\eta_0 = 1 - 2\exp\left(\frac{-2T_c}{T}\right). \tag{13}$$

As seen in Fig. 4, the spontaneous polarization $P_a \sim \eta_0$ follows the $(T_c - T)^{1/2}$ power law down to about $T_c - 30$ K and the exponential law, Eq. (13) at low temperatures up to about 225 K. The longitudinal permittivity follows the Curie-Weiss law both in the ferroelectric phase down to $T_c - 30\,\mathrm{K}$ and in the paraelectric phase. The ratio of the corresponding Curie constants is the classical 1:2. The spontaneous and associated with the field E_a critical behavior of the model is thus as expected for the mean-field theory of the ferroelectric Ising-like systems [18].

For the properties of APHTZ associated with the field E_b, the ratio between J_{12} and J_{11} becomes relevant, and so does the dipole moment μ_b. The value of J_{12} can be determined from the difference between the thermodynamic potentials g, Eq. (6), of the fully ordered system in the FE-II and FE-I configurations ($T \to 0$, $\eta_1 \to 1$, and $\eta_2 \to -1$ or 1, respectively), recalculated per one molecule

$$\frac{g^{\mathrm{FE-II}} - g^{\mathrm{FE-I}}}{2} = \frac{J_{12}}{4} = \Delta E$$

and equated to the energy difference between the FE-II and FE-I states $\Delta E = 0.53$ meV/molecule, found by the DFT calculations [2]. We obtain that $J_{12}/k_{\mathrm{B}} \approx 24\,\mathrm{K}$. Correspondingly, $J_{11}/k_{\mathrm{B}} = 1676$ K. As one can see, $|J_{12}| \ll J_{11}$, i.e., the coupling between the sublattices is much weaker than within them.

The calculated [2] using the Berry phase formalism polarization P_a of the FE-I configuration is about 1.5 times larger than polarization P_b of the FE-II configuration. This number is basically the ratio of the lattice constants a/b [2], and it reflects the fact that the sublattice polarization vector is directed along the chains of the hydrogen bonds, i.e., along [110] or [1$\bar{1}$0]. In our calculations, we adopt the same ratio for μ_a/μ_b, resulting in $\mu_b = 2.2 \times 10^{-29}$ C m.

Unlike ε_a^{-1}, the inverse transverse permittivity ε_b^{-1} shown in Fig. 4 (right) remains finite at the transition point. The corresponding paraelectric Curie-Weiss temperature is $T_b^{\mathrm{CW}} = 413\,\mathrm{K}$, as dictated by Eq. (10). This type of behavior is consistent with the one obtained within the Kittel model [19] for AFE systems.

Having experimental data for the transition temperature as well as for the temperature dependences of the characteristics depicted in Fig. 4 is crucial for ascertaining the values of the fitting parameters, especially J_{11}.

As predicted, the field E_b switches the polarization in one of the sublattices in the AFE-like manner and induces the transition from FE-I to FE-II phase. This process is illustrated in Fig. 5. At low temperatures the switching is a first-order phase transition, at which P_b has an upward jump, whereas P_a falls precisely to zero. Double AFE-type P_b-E_b hysteresis loops are expected to be experimentally observed for the field E_b, as opposed to the already observed [2] single FE-type P_a-E_a ones for E_a.

The magnitudes of P_a and P_b jumps decrease with increasing temperature, until just below T_c, at $T^* = 423$ K, the transition becomes of the second order: the tricritical point occurs. At T^* the left-hand derivative dP_b/dE_b diverges as $E_b \to E^* - 0$, i.e., below the switching. Above T^*, only a barely discernible bend of the $P_b(E_b)$ curve can be observed; the corresponding permittivity curve $\varepsilon_b(E_b)$, however, has a

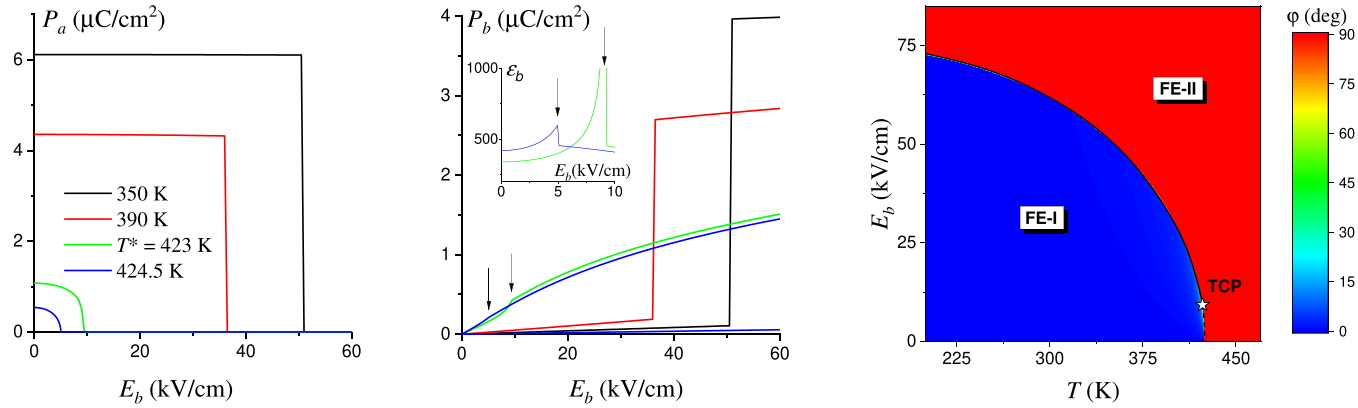


FIG. 5. Dependences of the polarization components P_a (left) and P_b (center) of APHTZ on the field E_b at different temperatures. The arrows indicate the bends in the $P_b(E_b)$ curves. The inset: the permittivity $\varepsilon_b = \varepsilon_0^{-1} dP_b/dE_b$ obtained by numerical differentiation of P_b as a function of E_b. (right) The T-E_b color contour plot of the angle $\varphi = \arctan P_b/P_a$ between the net polarization vector and the a axis. Solid and dashed lines: first and second order phase transitions, respectively; ☆: the tricritical point (T^*, E_b^*).

visible peak at that field (see the inset in Fig. 5). Above T_c, there is no spontaneous polarization P_a to be switched, so the field E_b simply induces some nonzero P_b. This is the typical behavior of an Ising type system with antipolar ordering [20].

The T-E_b phase diagram of APHTZ overlapped by the color contour plot of the angle $\varphi = \arctan P_b/P_a$ between the net polarization vector and the a axis is presented in Fig. 5. This angle is strictly 90° in the FE-II phase and predominantly small in the FE-I phase, except for a very narrow region near the transition line in the vicinity of the tricritical point. Thus, the switching, as expected according to the scheme in Fig. 3, is a 90° rotation of the net polarization.

As one can see, the temperature behavior of the switching field E_{sw} follows that of the spontaneous polarization P_a and order parameter η_0. This is not accidental. Thus, for the second-order transition (at temperatures between T^* and T_c) the temperature dependence of E_{sw} is determined by the power law

$$\mu_b E_{sw} \simeq J_{12}\sqrt{1-\frac{T}{T_c}} = \frac{J_{12}\eta_0}{\sqrt{3}}, \tag{14}$$

giving an explicit connection between the switching field and the spontaneous order parameter η_0 at these temperatures. Derivation of Eq. (14) and subsequently Eqs. (15) and (16) is given in Appendix.

For the first-order transitions below T^*, the connection between E_{sw} and η_0 is just as straightforward

$$\mu_b E_{sw} = \frac{J_{12}\eta_0}{2}. \tag{15}$$

Equations (14) and (15) have another obvious and intuitively clear physical meaning: the stronger is the coupling between the sublattices, the larger field is required to switch the polarization in one of them.

Finally, the temperature of the tricritical point is

$$T^* = T_c\left(1-\frac{1}{3}\frac{J_{12}}{J_{11}}\right). \tag{16}$$

The stronger are the intersublattice interactions J_{12} as compared to the intrasublattice J_{11}, the farther is the tricritical point from T_c. For the adopted values of J_{12} and J_{11} it yields $T^* = 423$ K, just as predicted by the direct calculations.

As one can see in Fig. 6, where the directly calculated switching fields are compared to those obtained within the presented above approximations, Eq. (15) for the first-order transitions is adequate in the whole temperature range below T^* up to the tricritical point. The switching field curve for the second-order transitions between T^* and T_c, obtained from Eq. (14), deviates from the exact results of Eq. (A2) only very slightly.

III. MPHTZ

The orthorhombic (space group *Pbca*) crystal structure of MPHTZ crystals is shown in Fig. 7. Unlike in APHTZ, here all hydrogen-bonded chains are parallel and go along the a axis without canting. It appears that there is a FE ordering within each chain and an AFE ordering of polarizations of different chains. Directions of the chain polarizations can

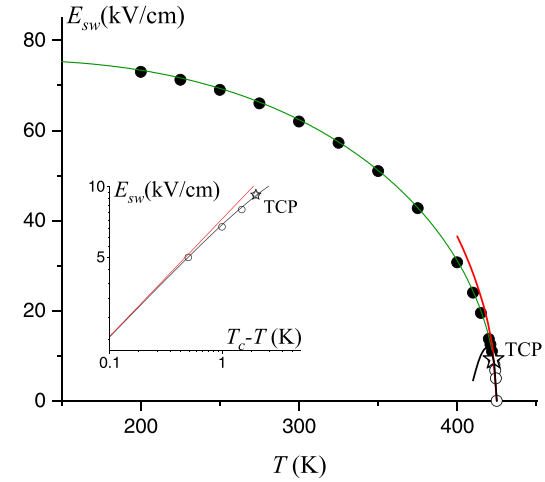


FIG. 6. The temperature dependences of the switching field E_{sw} in APHTZ. Symbols: direct calculations (○ and ●: the second and first-order phase transitions, respectively; ☆: the tricritical point); black lines: Eq. (A2); red lines: Eq. (14); green line: Eq. (15).

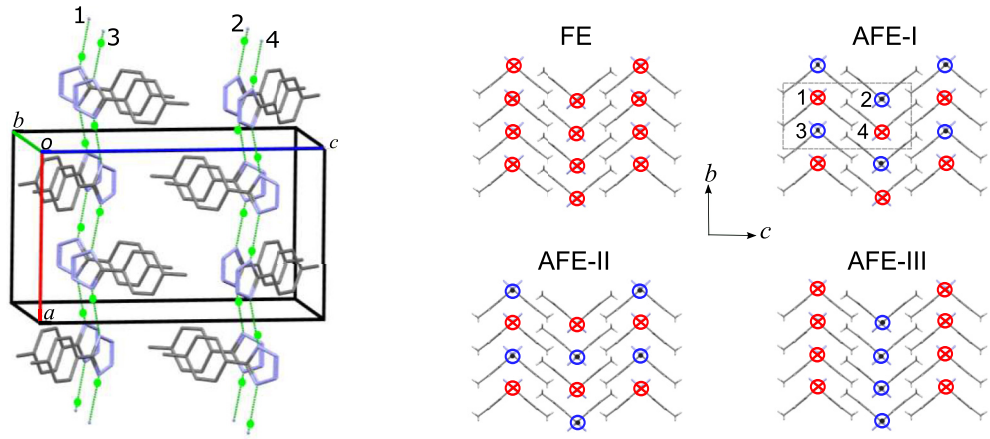


FIG. 7. (left) Crystal structure of MPHTZ in the AFE-I configuration, visualized [17] using the x-ray data of Ref. [2]. Hydrogen bonds, linking the tetrazole groups, are shown in green; the other hydrogen atoms are hidden for clarity; $s = 1,\ 2,\ 3,\ 4$ are the indexes of the sublattices. The off-center displacements of protons along the bonds are exaggerated. (right) Possible FE and AFE long-range configurations of MPHTZ (drawn after Ref. [2]). Polarizations in each chain are parallel to the a axis, perpendicular to the plane of the figure. The black dashed rectangle outlines the unit cell of the model.

alternate differently: in a checkerboard manner (configuration AFE-I in Fig. 7), from layer to layer along the b axis (layers parallel to the axis c, configuration AFE-II) or along the c axis (layers parallel to b, configuration AFE-III). According to the DFT calculations [2], configuration AFE-I has the lowest energy.

The proposed model is naturally chosen to consist of going along the a axis chains of Ising-like dipoles. The system is divided into four sublattices, as depicted in Fig. 7. The same pseudospin formalism is used, as in the previous Section, attributing the dipoles to the protons moving in the double-well potentials, to which the ionic displacements and switchable π bonds in the tetrazole rings are rigidly tied.

The model Hamiltonian includes pairwise long-range interactions between the dipoles, as well as the energy of their interactions with the longitudinal electric field E_a, which is expected to flip the sublattice polarization and induce the transition to the configuration FE

$$H = -\frac{1}{2}\sum_{s,s'=1}^{4}\sum_{ff'} J_{\substack{sf\\ s'f'}}\frac{\sigma_{sf}}{2}\frac{\sigma_{s'f'}}{2} - \mu_a E_a \sum_{s=1}^{4}\sum_{f}\frac{\sigma_{sf}}{2}. \quad (17)$$

The summations go over the four sublattices ($s = 1, 2, 3, 4$) and sites f belonging to the sublattice s. The combined index f includes the cell index, as well as the index of the site, belonging to the sth chain in this cell. Note that any notations introduced in this Section are relevant to MPHTZ crystals only.

For the sake of generality, we first consider this four-sublattice model with four nonequivalent chains in each cell, which at the proper choice of the interaction parameters can be reduced to any of the two-sublattice configurations AFE-I, AFE-II, AFE-III from Fig. 7. In this general model, there are four distinct order parameters $\eta_s = \langle\sigma_{sf}\rangle$. Applying the mean-field approximation leads to the following Hamiltonian:

$$H = NH_0' - \sum_{s=1}^{4}\sum_{f\in s} h_s\frac{\sigma_{sf}}{2}, \quad (18)$$

where N is the total number of dipoles in each sublattice,

$$H_0' = \frac{1}{8}\sum_{ss'=1}^{4} J_{ss'}\eta_s\eta_{s'},$$

and

$$h_s = \frac{1}{2}\sum_{s'=1}^{4} J_{ss'}\eta_{s'} + \mu_a E_a. \quad (19)$$

The interaction constants $J_{ss'} = \sum_{f'\in s'} J_{\substack{sf\\ s'f'}}$ have the following orthorhombic symmetry

$$J_{ss'} = J_{s's}, \quad J_{11} = J_{22} = J_{33} = J_{44};$$
$$J_{12} = J_{34}, \quad J_{13} = J_{24}, \quad J_{14} = J_{23}.$$

From here the thermodynamic potential (per *four* molecules) is obtained straightforwardly

$$g = \frac{G}{N} = H_0' - \frac{1}{\beta}\sum_{s=1}^{4}\ln 2\cosh\frac{\beta h_s}{2}. \quad (20)$$

The form of equations for the order parameters η_s is identical to that in APHTZ, Eq. (7). Finally, the longitudinal polarization is

$$P_a = \frac{\mu_a}{2v}(\eta_1 + \eta_2 + \eta_3 + \eta_4), \quad (21)$$

where $v = 784$ Å^3 is the crystal volume per four formula units [2].

As in the APHTZ case, it is obligatory that $J_{11} > 0$ to ensure the FE ordering and absence of modulation within each separate chain (sublattice). The interaction constant J_{14} does not bring any new essential physics, but only increases the number of the model parameters. We put $J_{14} = 0$. The signs of J_{12} and J_{13} then solely determine the character of the AFE ordering amongst the chains: $J_{12} < 0$, $J_{13} < 0$ yield configuration AFE-I; $J_{12} > 0$, $J_{13} < 0$ configuration AFE-II; and $J_{12} < 0$, $J_{13} > 0$ configuration AFE-III.

Since configuration AFE-I has been found [2] to have the lowest energy, we shall put $J_{12} < 0$, $J_{13} < 0$. Under such a

choice, the sublattice polarizations alternate in a checkerboard pattern from one chain to the neighboring one, and the number of the order parameters reduces to two: $\eta_1 = \eta_4$ and $\eta_2 = \eta_3$ at $E_a \neq 0$, and to one, $\eta_1 = -\eta_2 \equiv \eta_0$ in the absence of the field. Since in this case only the sum $J_{12} + J_{13}$ enters all the expressions, for the sake of simplicity, we also take $J_{12} = J_{13}$, i.e., impose a tetragonal symmetry on the model. As usual, $\eta_A = (\eta_1 - \eta_2)/2$ and $\eta_F = (\eta_1 + \eta_2)/2$ can be considered as auxiliary AFE and FE order parameters, respectively.

The thermodynamic potential (per *two* molecules) can now be rewritten in exactly the same form as Eq. (6), with

$$H_0 = \tfrac{1}{8}\left[J_{11}\eta_1^2 + 4J_{12}\eta_1\eta_2 + J_{11}\eta_2^2\right],$$

and

$$h_1 = \frac{J_{11}\eta_1 + 2J_{12}\eta_2}{2} + \mu_a E_a,$$
$$h_2 = \frac{2J_{12}\eta_1 + J_{11}\eta_2}{2} + \mu_a E_a. \tag{22}$$

The proposed model for MPHTZ is thus reduced to the traditional two-sublattice AFE Ising model, whose thermodynamics has been thoroughly studied yet in Ref. [20] and is well known.

By differentiating the polarization $P_a = 2\mu_a\eta_F/v$, we find the longitudinal permittivity at zero bias field

$$\varepsilon_a = \frac{\beta\mu_a^2}{\varepsilon_0 v\bar{\varphi}_a}, \tag{23}$$

where

$$\bar{\varphi}_a = \frac{1}{1-\eta_0^2} - \frac{\beta(J_{11}+2J_{12})}{4}.$$

It is expected to remain finite at all temperatures. The Curie-Weiss law is obeyed in the paraelectric phase, with the Curie-Weiss temperature

$$T^{\mathrm{CW}} = \frac{J_{11}+2J_{12}}{4k_{\mathrm{B}}}. \tag{24}$$

The expressions for the predicted second-order phase transition temperature at zero bias field

$$T_{\mathrm{N}} = \frac{J_{11}-2J_{12}}{4k_{\mathrm{B}}}, \tag{25}$$

the temperature dependence of the field of switching to the FE phase

$$\mu_a E_{sw} = -J_{12}\eta_0 \tag{26}$$

for the first-order transitions at temperatures below T^* and

$$\mu_a E_{sw} \simeq -2J_{12}\sqrt{1-\frac{T}{T_{\mathrm{N}}}}, \tag{27}$$

for the second-order transitions above T^*, where the temperature of the tricritical point is

$$T^* = T_{\mathrm{N}}\left(1 + \frac{2}{3}\frac{J_{12}}{J_{11}}\right), \tag{28}$$

have been derived in Appendix. Equations (27) and (28) were obtained yet in Ref. [20].

Additionally, the same power law

$$\eta_0 = \sqrt{3\frac{T_{\mathrm{N}}-T}{T_{\mathrm{N}}}} \tag{29}$$

and exponential

$$\eta_0 = 1 - 2\exp\left(\frac{-2T_{\mathrm{N}}}{T}\right) \tag{30}$$

approximations of the spontaneous order parameter at temperatures close to the phase transition and to saturation are obtained for the case of the antiferroelectric MPHTZ, as in the previous Section for APHTZ.

The fitting procedure for MPHTZ is similar to that for APHTZ. The parameters $\mu_a = 5 \times 10^{-29}$ C m and $J_{12}/k_{\mathrm{B}} = -41.6$ K are chosen to obtain the best fit to the experimental dependence [2] of polarization P_a on the field E_a at 300 K, in particular, to the values of the switching field and polarization above the switching. The parameter $J_{11}/k_{\mathrm{B}} = 1600$ K is then chosen to set T_{N} above the experimentally proven [2] minimal stability limit of the AFE phase, 410 K. At the adopted values of J_{11} and J_{12}, the theoretical T_{N} is 421 K. Again, $|J_{12}| \ll J_{11}$, i.e., the coupling between the sublattices is much weaker than within them.

Alternatively, the intersublattice interaction parameter J_{12} can be determined according to the same scheme as for APHTZ, by equating the energy difference between the fully ordered FE ($\eta_1 \to 1$, $\eta_2 \to 1$) and AFE-I ($\eta_1 \to 1$, $\eta_2 \to -1$) states found from the model thermodynamic potential to $\Delta E = 1.78$ meV/molecule [2], obtained by the DFT calculations

$$\frac{g^{\mathrm{FE}} - g^{\mathrm{AFE-I}}}{2} = -\frac{J_{12}}{2} = \Delta E.$$

This yields basically the same value of $J_{12}/k_{\mathrm{B}} = -41.3$ K, as that found by fitting to the experimental $P_a(E_a)$ dependence. This agreement between the two independent estimates of J_{12} is an important evidence in favor of the model's validity.

The temperature dependence of the spontaneous order parameter η_0 is presented in Fig. 8. The power law and exponential approximations (29) and (30) are adequate down to $T_{\mathrm{N}} - T \simeq 25$ K and up to 210 K, respectively. The temperature curve of the inverse permittivity $\varepsilon_a^{-1}(T)$ is as expected from the Kittel model: it follows the Curie-Weiss law and remains finite at the transition point. The paraelectric Curie-Weiss temperature is $T^{\mathrm{CW}} = 379$ K, as follows from Eq. (24).

The field-induced switching from AFE to FE phase is typical for uniaxial antiferroelectrics at the small negative $J_{12}/(J_{11} - J_{12})$ ratio [20], see also [21]. At lower temperatures, the switching is a first-order phase transition. With increasing temperature, the polarization jump decreases and eventually transforms to a bend in the $P_a(E_a)$ curve (cf. the $P_b(E_b)$ curves, Fig. 5), the bevahior indicative of the presence of the tricritical point.

This agrees with the T-E_a phase diagram presented in Fig. 8. This diagram is topologically identical to that of APHTZ for the transverse field E_b (Fig. 5). However, here the tricritical point occurs farther from T_{N}, at 413 K, which agrees with Eq. (28), and the values of the switching fields are also overall larger than those obtained for APHTZ. These

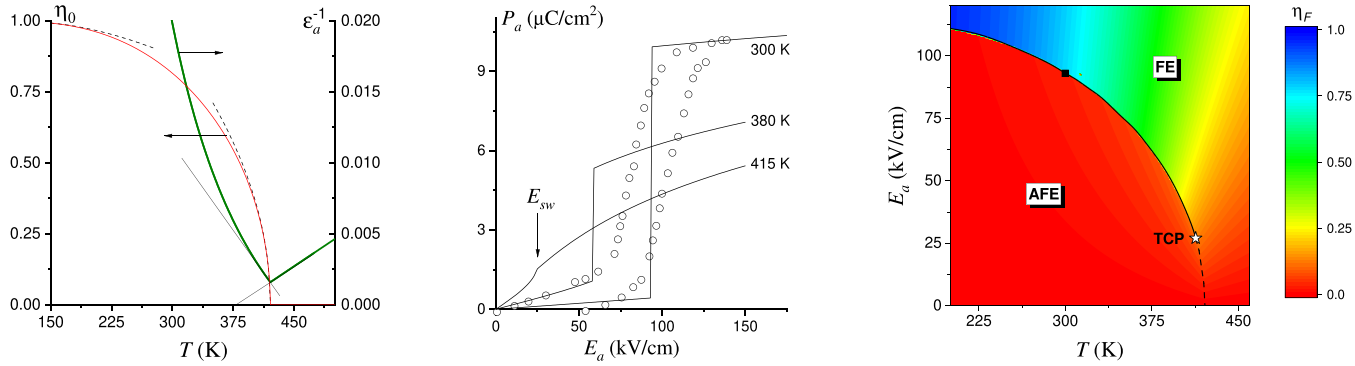


FIG. 8. (Left) Dependences of the spontaneous order parameter η_0, inverse dielectric permittivity ε_a^{-1} of MPHTZ on temperature. Solid lines: the theory; dashed lines: η_0 approximated according to Eqs. (29) and (30). (Center) Dependences of the net polarization P_a on the field E_a at different temperatures. ○: experimental data [2] for 300 K. (Right) The T-E_a color contour plot of the FE order parameter η_F. Solid and dashed lines: the first and second order phase transitions, respectively; ☆: the tricritical point (T^*, E_a^*); ■: experimental point [2].

differences are attributed to the weaker intersublattice interactions in APHTZ, inferred from the smaller energy difference between the states below and above the switching [2], and follow directly from Eqs. (14)–(16) and (26)–(28).

Adequacy of the approximations (26)–(28) is verified in Fig. 9. All conclusions made in the previous Section from the similar graph of the switching field for APHTZ, Fig. 6, remain valid for MPHTZ as well.

Even though the present theory considers only the equilibrium states of the system, and therefore, there is no hysteresis at the first-order phase transition switching, we still can draw some conclusions about the stored and recoverable energy densities for the studied crystals, the primary characteristics of a system that potentially can be used for energy storage. By definition, these densities are given by the areas between the polarization axis and, respectively, right/left branches of the $P_a(E_a)$ hysteresis loop at $E_a > 0$ (forward/backward transitions). The area $W = \int E_a dP_a$ between the theoretical $P_a(E_a)$ curve and the polarization axis can then serve as the lower and upper limit estimates of the actual stored and recoverable energy densities.

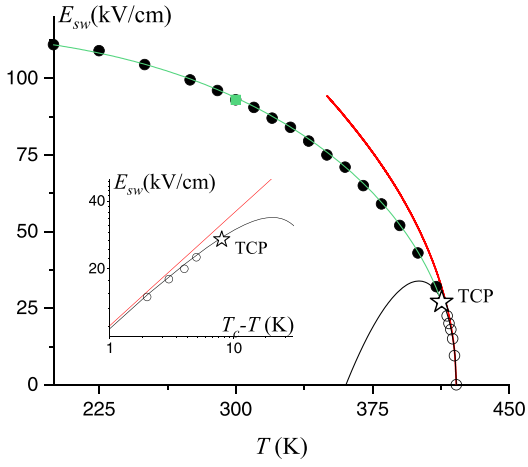


FIG. 9. The temperature dependences of the switching field E_{sw} in MPHTZ. Symbols: direct calculations (○ and ●: the second and first order phase transitions, respectively; ☆: the tricritical point); black lines: Eq. (A6); red lines: Eq. (27); green line: Eq. (26). ■: the experimental point [2].

It is obvious from Fig. 8 that at the same value of the maximal applied field ($E_{\max} > E_{sw}$), this area is the largest if there is no significant increase of polarization below and above the switching, i.e., the corresponding dielectric permittivity is small, and the switching is just polarization flipping in one of the sublattices. In other words, the working temperature should be far from T^*, where the permittivity diverges (see the inset to Fig. 5), and also far from T_c. We then estimate the optimal recoverable energy density by approximating the $P_a(E_a)$ curve by a step-like increase of polarization from zero to $\Delta P_a = 2\mu_a\eta_0/v$ at E_{sw}. Using Eq. (26), we obtain that

$$W = E_{sw}\Delta P_a = -\frac{2J_{12}\eta_0^2}{v}. \tag{31}$$

With $\eta_0 = 0.815$ at 300 K it yields $W = 0.966$ J/cm^3 for MPHTZ, in a good agreement with the experimental [2] stored energy density value 1.044 J/cm^3.

Counterintuitively, W does not depend on the value of the dipole moment μ_a, which is canceled out in the $E_{sw}\Delta P_a$ product. Larger intersublattice interactions J_{12} increase W, provided that the ratio J_{12}/J_{11} is still small enough for the tricritical point to be far from the working temperature [see Eq. (28)]. The more the system is ordered at zero field (the closer $|\eta_0|$ is to 1), the larger is W. Maximal possible W is therefore $W_{\max} = -2J_{12}/v$ or 1.45 J/cm^3 for a fully ordered MPHTZ.

IV. CONCLUDING REMARKS AND OUTLOOK

We propose pseudospin models, which reproduce the essential structures of the ordering subsystem in the two crystals of the phenyltetrazole family, APHTZ and MPHTZ, and, hopefully, can qualitatively and quantitatively correctly describe their temperature and electric field behavior. A good agreement with the experimental data is obtained.

However, the available data are still not sufficient to make definite conclusions about the adequacy of the developed approach. First, the obtained critical behavior of the models (the second order phase transition, the $\sqrt{T_c - T}$ dependence of the order parameter, the Curie-Weiss law for the permittiv-

ities, the T-E phase diagrams with a tricritical point) is as expected for the Ising-type systems treated in the mean-field approximation. That needs to be confirmed experimentally. Second, though the number of the used free parameters is absolutely minimal, there is still a certain degree of uncertainty (in particular for the values of the intrasublattice interaction parameter J_{11}), caused by the severe lack of experimental data to base the fitting on. Therefore measurements of the temperature dependences of spontaneous polarization, dielectric permittivities, polarization switching, eventual determination of temperatures and order of the phase transitions to the paraelectric phase are absolutely necessary in order to test the model validity and ascertain the values of the free parameters. It may also transpire that further sophistications of the models are required, like employing the two-particle cluster approximation for the intrachain correlations.

The processes of polarization switching by external electric field are studied in detail. MPHTZ behaves like a classical uniaxial AFE: the field-induced net polarization is confined to this axis, and the classical switching with double P-E hysteresis loops is observed [2]. APHTZ, a canted FE, is different: it behaves like a FE, when spontaneous or associated with the longitudinal field E_a applied along the a axis characteristics are concerned, and like an AFE, when associated with a transverse field E_b, perpendicular to the axis of spontaneous polarization, characteristics are concerned. Flipping one of the sublattice polarizations by 180° by the transverse field leads to a 90° rotation of the net polarization. In addition to the single FE loop observed [2] for the longitudinal field E_a, one should also observe a double loop for the transverse field E_b. To investigate the effect of changing the external field direction, i.e., combining the longitudinal E_a and transverse E_b bias fields, on the polarization rotation in APHTZ could be particularly interesting.

APHTZ crystals may also present an academically interesting case as far as the electrocaloric effect in them is concerned. Commonly, in FEs it is positive, $dT/dE > 0$, whereas in AFEs it can be positive or negative, $dT/dE < 0$, in different fields or temperature domains [22,23]. It would be interesting to determine the sign of the electrocaloric effect in APHTZ, where the FE ordering along the a axis coexists with the AFE ordering along the b axis, and the situation can be reversed by the field E_b.

The parent PHTZ compound, identified as a mixture of two different AFE phases with close energies [2], is intriguing. Judging by the shape of the double hysteresis loops in it, the switching fields of the two phases must also be very close. The present model approach can explain that, as it appears that these two phases will be indistinguishable in the mean-field approximation, thus having identical energies and switching fields. More detailed calculations are in order.

DATA AVAILABILITY

The data that support the findings of this article are openly available [24].

APPENDIX

The typical dependences of the order parameters in APHTZ in the vicinity of the switching induced by the electric field E_b are depicted in Fig. 10. Note that just above the transition $\eta_1^+ = -\eta_2^+$. Using Eqs. (7) it can also be shown that in the linear over E_b approximation, which as seen in Fig. 10 is well appropriate for $T < T^*$, we have

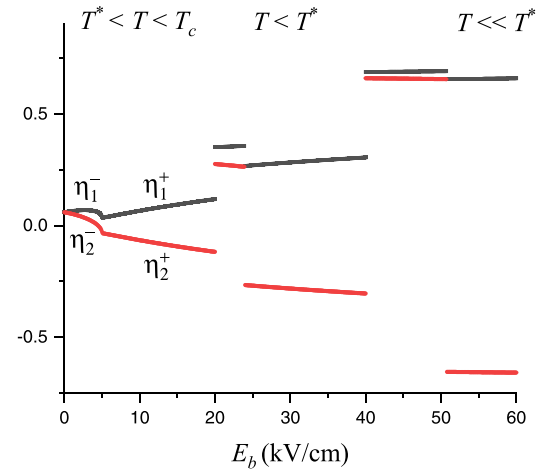


FIG. 10. The field dependences of the order parameters in APHTZ at different temperatures: 424.5 K ($T^* < T < T_c$), 410 K ($T < T^*$), and 350 K ($T \ll T^*$).

$$\eta_1^- + \eta_2^- = 2\eta_0, \tag{A1}$$

where η_0 is the spontaneous order parameter in the FE-I phase.

In order to obtain the temperature dependence of the switching field for the first order transitions (below T^*), one has to equate the thermodynamic potentials, Eq. (6), for the two phases just below and above the transition, i.e., at $\eta_1 = \eta_1^-$, $\eta_2 = \eta_2^-$ and at $\eta_1 = -\eta_2 = \eta_1^+$:

$$-\frac{1}{\beta}\ln\frac{\cosh(\beta h_1^-/2)\cosh(\beta h_2^-/2)}{\cosh^2(\beta h_1^+/2)} = H_0^+ - H_0^-,$$

where H_0 and $h_{1,2}$ are given by Eqs. (3) and (4), respectively. In a linear over E_b approximation, we obtain that

$$\mu_b E_{sw} = 2\frac{H_0^+ - H_0^- + \beta^{-1}\ln\frac{\cosh a\cosh b}{\cosh^2 c}}{2\tanh c - \tanh a + \tanh b},$$

where $a = \beta(J_{11}\eta_1^- + J_{12}\eta_2^-)/4$, $b = \beta(J_{12}\eta_1^- + J_{11}\eta_2^-)/4$, and $c = \beta(J_{11} - J_{12})\eta_1^+/4$. At small deviations of the order parameters from 1 and using Eqs. (13) and (A1), it leads to the following equation:

$$\mu_b E_{sw} = \frac{J_{12} + 2\beta^{-1}(1-\eta_0)[1-\exp(\beta J_{12})]}{2[1-(1-\eta_0)[1-\exp(\beta J_{12})]]}.$$

Expanding it in series and retaining up to the linear terms in βJ_{12} and $1-\eta_0$, we obtain a remarkably simple final expression for the switching field, Eq. (15). As one can see in Fig. 6, despite all the used approximations, E_{sw} given by this expression agrees with the results of direct calculations surprisingly well.

Curiously, Eq. (15) can be obtained in a much simpler way, if one uses an empirical fact that at the switching point $\eta_2^- \simeq \eta_1^+$ at low temperatures (see Fig. 10). Equating h_2^- to h_1^+ and taking into account Eq. (A1), one immediately arrives at Eq. (15).

To obtain the temperature dependence of the switching field above T^*, we use the condition that the derivative dP_a/dE_a diverges at the second-order phase transition point. Taking into account the fact that at the transition $\eta_1 = -\eta_2 \equiv \eta_{sw}$ (see Fig. 10) and calculating the derivative at $E_b \neq 0$, we obtain that

$$\eta_{sw} = \sqrt{1 - \frac{T}{T_c}}.$$

Substituting it into Eq. (7), we find an exact expression for the switching field above T^*

$$\frac{\mu_b E_{sw}}{k_B} = 2T \operatorname{arctanh}\sqrt{1 - \frac{T}{T_c}} - \left(2T_c - \frac{J_{12}}{k_B}\right)\sqrt{1 - \frac{T}{T_c}}. \tag{A2}$$

At temperatures close to T_c, it can be approximated by Eq. (14).

The temperature of the tricritical point T^* can be found by following the scheme suggested in Ref. [20]. We introduce auxiliary order parameters $\eta_I = (\eta_1 + \eta_2)/2$ and $\eta_{II} = (\eta_1 - \eta_2)/2$ and rewrite Eqs. (7) as

$$\frac{2\eta_I}{1 + \eta_I^2 - \eta_{II}^2} = \tanh\left[\beta\mu_b E_b + \left(2\frac{T_c}{T} - \beta J_{12}\right)\eta_I\right],$$
$$\frac{2\eta_{II}}{1 - \eta_I^2 + \eta_{II}^2} = \tanh\left[2\frac{T_c}{T}\eta_{II}\right]. \tag{A3}$$

Since the tricritical point (T^*, E_b^*) is the terminating point of the second-order transition line, at this point $\eta_{II} = 0$ and $\eta_I = \eta_{sw}$. We then expand Eqs. (A3) at $T = T^*$ in the vicinity of E_b^* with $\Delta E = E_b - E_b^* < 0$, η_{II}, and $\Delta\eta = \eta_I - \eta_{sw}$ as small parameters. The coordinates of the tricritical point are found from the condition that the left-hand derivative $d\eta_{II}/dE_b$ diverges, or that $\Delta E/\Delta\eta = 0$. Some lengthy algebra leads to yet another remarkably simple expression, Eq. (16).

The typical dependence of the order parameters in MPHTZ in the vicinity of the switching, depicted in Fig. 11, is different from that in APHTZ. Above the transition $\eta_F = \eta_1^+ = \eta_2^+$, and it can be shown that

$$\eta_A^- = \eta_1^- - \eta_2^- = 2\eta_0 \tag{A4}$$

is obeyed instead of Eq. (A1).

To find the values of the FE order parameter at the second-order transition switching η_F^{sw}, we assume that in addition to the bias E_a, a hypothetical measuring staggered field E_{st} is applied, so that $h_1 \to h_1 + \mu_{st}E_{st}$, and $h_2 \to h_2 - \mu_{st}E_{st}$ [h_i are given in Eq. (22)]. For the point, where the linear response of the AFE order parameter η_A to the field E_{st} diverges, one gets

$$\eta_F^{sw} = \sqrt{1 - \frac{T}{T_N}}, \tag{A5}$$

where the transition temperature T_N at zero bias field, at which $\eta_F^{sw} = 0$, is given by Eq. (25).

In the same manner as described above for the case of APHTZ, we obtain

$$\frac{\mu_a E_{sw}}{k_B} = 2T \operatorname{arctanh}\sqrt{1 - \frac{T}{T_N}} - 2\left(T_N + \frac{J_{12}}{k_B}\right)\sqrt{1 - \frac{T}{T_N}}, \tag{A6}$$

instead of Eq. (A2) for the switching fields above the tricritical point, Eq. (27) as its approximation, as well as expression (28) for the temperature of the tricritical point and Eq. (27) for the switching fields below it.

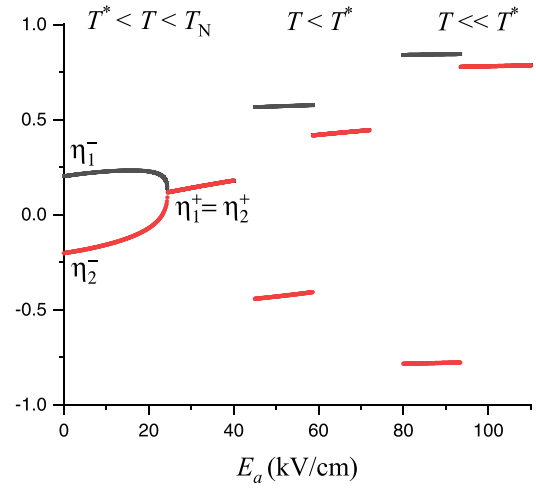


FIG. 11. The field dependences of the order parameters in MPHTZ at different temperatures: 415 K ($T^* < T < T_N$), 380 K ($T < T^*$), and 300 K ($T \ll T^*$).

[1] S. Horiuchi, H. Minemawari, J. Tsutsumi, S. Ishibashi, Field-effect crystal engineering in proton–π-electron correlated systems, Crystals **15**, 736 (2025).

[2] S. Horiuchi, H. Minemawari, and S. Ishibashi, Competition of polar and antipolar states hidden behind a variety of polarization switching modes in hydrogen-bonded molecular chains, Mater. Horiz. **10**, 2149 (2023).

[3] S. Horiuchi, R. Kumai, and S. Ishibashi, Strong polarization switching with low-energy loss in hydrogen-bonded organic antiferroelectrics, Chem. Sci. **9**, 425 (2018).

[4] A. P. Moina, Polarization rotation by external electric field in the two-dimensional antiferroelectric squaric acid $H_2C_4O_4$, Phys. Rev. B **103**, 214104 (2021).

[5] A. P. Moina, Influence of external field direction on polarization rotation in antiferroelectric squaric acid $H_2C_4O_4$, Condens. Matter Phys. **24**, 43703 (2021).

[6] S. Horiuchi and S. Ishibashi, Large polarization and record-high performance of energy storage induced by a phase change in organic molecular crystal, Chem. Sci. **12**, 14198 (2021).

[7] A. P. Moina, Effects of diagonal strains and H-bond geometry in antiferroelectric squaric acid crystals, Condens. Matter Phys. **23**, 33704 (2020).

[8] R. Blinc, On the isotopic effects in the ferroelectric of crystals with short hydrogen bonds, J. Phys. Chem. Solids **13**, 204 (1960).

[9] P. G. de Gennes, Collective motions of hydrogen bonds, Solid State Commun. **1**, 132 (1963).

[10] V. G. Vaks, N. E. Zein, and B. A. Strukov, On the theory of ferroelectrics of KH_2PO_4-KDP type, Phys. Stat. Sol. (a) **30**, 801 (1975).

[11] M. Tokunaga, Models of the phase transition in KDP type ferroelectrics, Ferroelectrics **1**, 195 (1970).

[12] I. R. Zachek and R. R. Levitskii, Relaxation dynamics of deuterated ferroelectric orthophosphates, Theor. Math. Phys. **43**, 364 (1980).

[13] I. V. Stasyuk, R. R. Levitskii, and A. P. Moina, External pressure influence on ferroelectrics and antiferroelectrics of the KH_2PO_4 family: A unified model, Phys. Rev. B **59**, 8530 (1999).

[14] A. V. de Carvalho and S. R. Salinas, Theory of the phase transition in the quasi-one-dimensional hydrogen-bonded ferroelectric crystal $PbHPO_4$, J. Phys. Soc. Jpn. **44**, 2383 (1978).

[15] I. R. Zachek, Y. Shchur, R. R. Levitskii, and O. B. Bilenka, On thermodynamic and dielectric properties of $PbHPO_4$ and $PbHAsO_4$ crystals, Phys. B: Condens. Matter **452**, 152 (2014).

[16] I. R. Zachek, Y. Shchur, R. R. Levitskii, and A. S. Vdovych, Thermodynamic properties of ferroelectric $NH_3CH_2COOH \cdot H_2PO_3$ crystal, Phys. B: Condens. Matter **520**, 164 (2017).

[17] C. F. Macrae, I. Sovago, S. J. Cottrell, P. T. A. Galek, P. McCabe, E. Pidcock, M. Platings, G. P. Shields, J. S. Stevens, M. Towler, and P. A. Wood, Mercury 4.0: From visualization to analysis, design and prediction, J. Appl. Cryst. **53**, 226 (2020).

[18] M. E. Lines and A. M. Glass, *Principles and Applications of Ferroelectrics and Related Materials* (Clarendon Press, Oxford, 1977).

[19] C. Kittel, Theory of antiferroelectric crystals, Phys. Rev. **82**, 729 (1951).

[20] R. Bidaux, P. Carrra, and B. Vivet, Antiferromagnetisme dans un champ magnetique I. Traitement de champ moleculaire, J. Phys. Chem. Solids **28**, 2453 (1967).

[21] P. Tolèdano and M. Guennou, Theory of antiferroelectric phase transitions, Phys. Rev. B **94**, 014107 (2016).

[22] A. Grünebohm, Y.-B. Ma, M. Marathe, B.-X. Xu *et al.*, Origins of the inverse electrocaloric effect, Energy Technol. **6**, 1491 (2018).

[23] A. P. Moina, Negative/positive electrocaloric effect in antiferroelectric squaric acid, J. Appl. Phys. **133**, 094101 (2023).

[24] A. Moina, Phase transition and polarization switching in quasi-one-dimensional ferroelectrics of phenyltetrazole family, Mendeley Data, V2 (2025), doi:10.17632/8tb356ydyh.2.